Organic & Biomolecular Chemistry

Accepted Manuscript

This article can be cited before page numbers have been issued, to do this please use: S. Yamada, M. Morita, T. Agou, T. Kubota, T. Ichikawa and T. Konno, *Org. Biomol. Chem.*, 2018, DOI: 10.1039/C8OB01497C.

ROYAL SOCIETY OF CHEMISTRY

rsc.li/obc

View Article Online
DOI: 10.1039/C8OB01497C

Journal Name

ARTICLE

Thermoresponsive luminescent properties of polyfluorinated bistolane-type light-emitting liquid crystals

Received 00th January 20xx,
Accepted 00th January 20xx

DOI: 10.1039/x0xx00000x

www.rsc.org/

Shigeyuki Yamada,*[a] Masato Morita,[a] Tomohiro Agou,[b] Toshio Kubota,[b] Takahiro Ichikawa,[c] and Tsutomu Konno[a]

We developed and characterized four polyfluorinated bistolane derivatives. These compounds, which possess either two alkoxy substituents or an alkoxy group and a bromine atom in their two molecular terminals, were synthesized from readily available 4-alkoxy-1-ethynylbenzene with a facile three-step procedure. Their thermodynamic and photophysical properties were evaluated in detail, and they were found to display both liquid-crystalline (LC) and photoluminescence properties. Remarkably, the photoluminescence behaviors dramatically changed during the thermal phase transition between the crystal and LC phases. Thus, these polyfluorinated bistolanes may be promising candidate for the thermoresponsive luminous molecules.

Introduction

Liquid crystals are an important class of soft materials with great potentials in various fields including displays,[1] optical communications,[2] as well as biomaterials,[3] because liquid-crytalline (LC) molecules have characteristics between anisotropic crystalline and fluidic liquid states. Various mesophase structures can be formed in the LC phases and convert into each other under external stimuli. Therefore, LC molecules can change their aggregated structures in condensed phase through phase transition.

It is well known that photophysical properties such as UV-Vis absorption and photoluminescence (PL) are quite sensitive to the molecular structure formed in both dispersed and aggregated systems, i.e., a slight modulation of the molecular structure can significantly alter the photophysical properties.[4–6] Owing to the intriguing optical characteristics of such luminous molecules, there is considerable interest in developing novel light-emitting molecules with switchable luminescent characteristics by an external stimulus, e.g., pH,[7] metal ions,[8] termperature,[9] and mechanical stress.[10] Their potential applications in luminescent sensing or detection have already propelled extensive studies of new, efficient, and stimuli-responsive luminescent materials.

Over the last few years, our group has examined novel multi-color PL molecules, by controlling the electron density distribution through precise tuning of the electronic nature of the substituents or using thermal phase transition of the LC molecules to vary the aggregated structures. We have previously reported two light-emitting LC molecules with a polyfluorinated bistolane scaffold **1aA** and **1bA** (Figure 1a).[11] Interestingly, by slight modulation of the chemical structure, the PL behaviour of polyfluorinated bistolane analogues is sensitive to their electronic structures or aggregated structures.[5a,11,12]

Here, to gain deep insight into these light-emitting LC materials, we synthesized polyfluorinated bistolane derivartives with various substituents at the longitudinal molecular terminals (Figure 1b), in order to systematically alter the electron density distribution or molecular packing structure. The photophysical and thermodynamic characteristics of the resultant molecules were examined in detail.

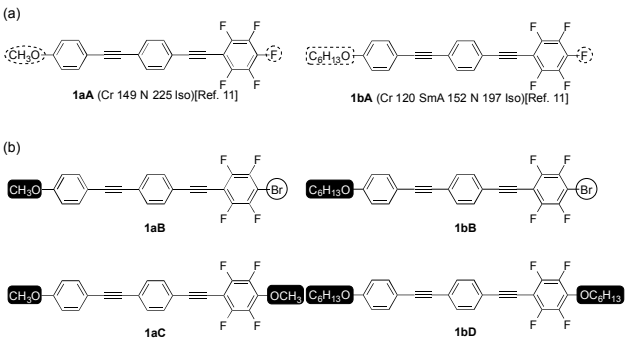

[a] Faculty of Molecular Chemistry and Engineering, Kyoto Institute of Technology, Matsugasaki, Sakyo-ku, Kyoto 606-8585, Japan. E-mail: syamada@kit.ac.jp
[b] Department of Quantum Beam Science, Graduate School of Science and Engineering, Ibaraki University, 4-12-1 Nakanarusawa, Hitachi, Ibaraki 316-8511, Japan.
[c] Department of Biotechnology, Tokyo University of Agriculture and Technology, Nakacho 2-24-1, Koganei, Tokyo 185-8588, Japan.

†Electronic Supplementary Information (ESI) available: Details of synthetic procedures, characterization, and NMR spectra (^{1}H, ^{13}C, and ^{19}F) for the polyfluorinated bistolanes **1**. Crystallographic details for **1bA** and **1aC**, Cartesian coordinates for calculated structure of **1** in the ground and excited states, results for powder X-ray diffraction measurement, DSC thermograms, UV-Vis spectra, photoluminescence spectra in dilute solution, excitation and PL spectra in crystal for the present bistolanes. See DOI: 10.1039/x0xx00000x

View Article Online
DOI: 10.1039/C8OB01497C

Figure 1. Chemical structures of (a) previously reported fluorinated bistolanes **1aA** and **1bA** in Ref.11, and (b) newly synthesized bistolanes reported in this study (**1aB**–**C**, **1bB**, and **1bD**).

Four polyfluorinated bistolanes synthesized in this study showed LC as well as PL characteristics, and their behavior changes depending on the structures of molecular aggregates formed through thermal phase transition. In this paper, we discuss the properties of the polyfluorinated bistolanes in connection with the LC and PL behaviors.

Experimental

General

^{1}H- and ^{13}C-NMR spectra were measured with a Bruker AVANCE III 400 NMR spectrometer (^{1}H: 400 MHz and ^{13}C: 100 MHz) in chloroform-*d* ($CDCl_3$) solution and the chemical shifts are reported in parts per million (ppm) using the residual proton in the NMR solvent. ^{19}F-NMR (376 MHz) spectra were measured with a Bruker AVANCE III 400 NMR spectrometer in $CDCl_3$ solution with $CFCl_3$ (δ_F = 0 ppm) as internal standard. Infrared spectra (IR) were determined in a KBr method with a JASCO FT/IR-4100 type A spectrometer; all spectra were reported in wavenumber (cm^{-1}). High resolution mass spectra (HRMS) were recorded on a JEOL JMS-700MS spectrometer using fast atom bombardment (FAB) methods. All reactions were carried out using dried glassware with a magnetic stirrer bar. All chemicals were of reagent grade and where necessary were purified in the usual manner prior to use. Column chromatography was carried out on silica gel (Wako-gel® 60N, 38–100 μm) and TLC analysis was performed on silica gel TLC plates (Merck, Silica gel 60F_{254}).

Synthesis

Polyfluorinated bistolane derivatives (**1aB**–**C**, **1bB**, and **1bD**) were prepared from (4-alkoxyphenyl)acetylene **2** according to the procedure in Scheme 1. A typical synthetic procedure for the final step to prepare **1** is described below. The molecular structures of bistolane **1** obtained were well characterized by spectroscopic analyses, like ^{1}H, ^{13}C, and ^{19}F NMR, infrared (IR), and high resolution mass spectrometry (HRMS). The NMR spectra indicate that the products were sufficiently pure for evaluating their LC and PL properties.

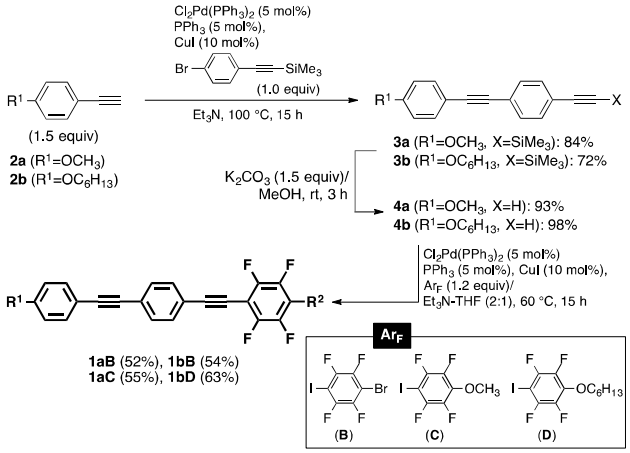

Scheme 1. Synthetic pathway for the polyfluorinated bistolanes **1aB–C**, **1bB**, and **1bD**.

Typical procedure for the preparation of 1-bromo-2,3,5,6-tetrafluoro-4-[[4-(4-methoxyphenyl)ethynyl]phenyl]ethynyl-benzene (1aB)

Et_3N (15 mL) and THF (5 mL) were added to a mixture of $Cl_2Pd(PPh_3)_2$ (53 mg, 0.042 mmol), PPh_3 (11 mg, 0.042 mmol), 4-[2-(4-methoxyphenyl)ethyn-1-yl]phenylacetylene (**4a**) (0.20 g, 0.85 mmol),[11] 1-bromo-2,3,5,6-tetrafluoro-4-iodobenzene (0.36 g, 1.02 mmol),[13] and CuI (16 mg, 0.084 mmol). The mixture was stirred at 60 °C (bath temp.) for 15 h. After removal of the solvent using a rotary evaporator, the crude product was extracted with AcOEt and washed with saturated aqueous NH_4Cl solution (three times). The organic layer was dried over anhydrous Na_2SO_4, filtered, and concentrated in vacuo. The resultant solid was purified by silica-gel column chromatography (eluent: hexane/CH_2Cl_2 = 3/1), providing the desired product (**1aB**, 0.20 g, 0.44 mmol) in 52% yield as a white solid. This product was recrystalized by slow evaporation from CH_2Cl_2/MeOH (1/1) to obtain the title compound in crystal.

1-Bromo-2,3,5,6-tetrafluoro-4-[[4-(4-methoxyphenyl)ethynyl]-phenyl]ethynylbenzene (1aB)

Yield: 52% (white solid); m.p.: 192 °C determined by DSC; ^{1}H-NMR ($CDCl_3$): δ3.84 (s, 3H), 6.89 (d, *J* = 8.8 Hz, 2H), 7.48 (d, *J* = 8.8 Hz, 2H), 7.52 (ABq, *J* = 8.4 Hz, 2H), 7.56 (ABq, *J* = 8.4 Hz, 2H); ^{19}F NMR ($CDCl_3$, $CFCl_3$): δ–133.64 (dd, *J* = 21.8, 9.4 Hz, 2F), –133.67 (dd, *J* = 21.8, 9.8 Hz, 2F); ^{13}C NMR ($CDCl_3$): δ55.3, 75.5 (t, *J* = 3.7 Hz), 87.6, 92.3, 100.6 (t, *J* = 22.7 Hz), 102.2 (t, *J* = 3.7 Hz), 104.2 (t, *J* = 16.2 Hz), 114.1, 114.9, 120.7, 125.2, 131.4, 131.8, 133.2, 144.9 (ddt, *J* = 247.2, 14.7, 3.6 Hz), 146.7 (ddt, *J* = 254.5, 14.0, 4.3 Hz), 159.9; IR (KBr): ν 3075, 2976, 2846, 2212, 1518, 1484, 1246, 1027, 967, 837 cm^{-1}; HRMS (FAB+) *m/z* $[M]^+$ calcd for $C_{23}H_{11}O^{79}BrF_4$: 457.9929; found: 457.9926.

2,3,5,6-Tetrafluoro-4-[4-[(4-methoxyphenyl)ethynyl]phenyl-ethynyl]anisole (1aC)

Yield: 55% (white solid); m.p.: 120 °C determined by DSC; ^{1}H-NMR ($CDCl_3$): δ3.84 (s, 3H), 4.13 (t, *J* = 1.6 Hz, 3H), 6.89 (d, *J* =

View Article Online
DOI: 10.1039/C8OB01497C

8.8 Hz, 2H), 7.48 (d, *J* = 8.8 Hz, 2H), 7.50 (ABq, *J* = 8.8 Hz, 2H), 7.54 (ABq, *J* = 8.8 Hz, 2H); ^{19}F-NMR ($CDCl_3$, $CFCl_3$): δ –137.75 (dd, *J* = 20.3, 7.9 Hz, 2F), –158.06 (dd, *J* = 20.7, 6.8 Hz, 2F); ^{13}C-NMR ($CDCl_3$): δ 55.3, 62.2 (t, *J* = 4.4 Hz), 75.7 (t, *J* = 4.4 Hz), 87.7, 92.0, 97.9 (t, *J* = 19.1 Hz), 99.9, 114.1, 115.0, 121.2, 124.6, 131.4, 131.7, 133.2, 138.9 (tt, *J* = 11.8, 2.9 Hz), 140.7 (ddt, *J* = 247.0, 14.5, 4.4 Hz), 147.2 (ddt, *J* = 240.5, 13.2, 4.3 Hz), 159.9; IR (KBr): ν 3014, 2964, 2836, 2210, 1605, 1428, 1285, 1122, 1027, 980, 833 cm^{-1}; HRMS: (FAB+) *m/z* $[M]^+$ calcd for $C_{24}H_{14}O_2F_4$: 410.0930; found: 410.0934.

1-Bromo-2,3,5,6-tetrafluoro-4-[4-[(4-hexyloxyphenyl)ethynyl]-phenylethynyl]benzene (1bB)

Yield: 54% (white solid); m.p.: 130 °C determined by DSC; ^{1}H-NMR ($CDCl_3$): δ 0.91 (t, *J* = 6.8 Hz, 3H), 1.32–1.37 (m, 4H), 1.42–1.51 (m, 2H), 1.79 (tt, *J* = 7.2, 6.8 Hz, 2H), 3.98 (t, *J* = 6.8 Hz, 2H), 6.88 (ABq, *J* = 8.4 Hz, 2H), 7.46 (ABq, *J* = 8.4 Hz, 2H), 7.51 (ABq, *J* = 8.8 Hz, 2H), 7.56 (ABq, *J* = 8.8 Hz, 2H); ^{19}F-NMR ($CDCl_3$, $CFCl_3$): δ –133.66 (dd, *J* = 21.8, 9.4 Hz, 2F), –135.69 (dd, *J* = 21.8, 10.9 Hz, 2F); ^{13}C-NMR ($CDCl_3$): δ 14.0, 22.6, 25.7, 29.2, 31.6, 68.1, 75.5 (t, *J* = 4.4 Hz), 87.5, 92.5, 100.6 (t, *J* = 22.7 Hz), 102.2 (t, *J* = 3.7 Hz), 104.2 (t, *J* = 18.3 Hz), 114.57, 114.61, 120.6, 125.2, 131.4, 131.8, 133.2, 144.9 (ddt, *J* = 262.6, 14.6, 4.4 Hz), 146.7 (ddt, *J* = 255.2, 14.7, 4.3 Hz), 159.6; IR (KBr): ν 3032, 2919, 2847, 2205, 1596, 1518, 1486, 1242, 1174, 967, 837 cm^{-1}; HRMS: (FAB+) *m/z* $[M]^+$ calcd for $C_{28}H_{21}O^{79}BrF_4$: 528.0712; found: 528.0706.

2,3,5,6-Tetrafluoro-4-[4-[(4-hexyloxyphenyl)ethynyl]phenyl-ethynyl]-1-hexyloxybenzene (1bD)

Yield: 63% (yellow solid); m.p.: 76 °C determined by DSC; ^{1}H-NMR ($CDCl_3$): δ 0.91(t, *J* = 7.2 Hz, 6H), 1.29–1.41 (m, 4H), 1.41–1.52 (m, 4H), 1.75–1.85 (m, 4H), 3.98 (t, *J* = 6.4 Hz, 2H), 4.27 (t, *J* = 6.4 Hz, 2H), 6.88 (ABq, *J* = 8.8 Hz, 2H), 7.46 (ABq, *J* = 8.8 Hz, 2H), 7.50 (ABq, *J* = 8.4 Hz, 2H), 7.53 (ABq, *J* = 8.4 Hz, 2H); ^{19}F-NMR ($CDCl_3$, $CFCl_3$): δ –138.48 (dd, *J* = 20.3, 7.9 Hz, 2F), –157.84 (dd, *J* = 20.3, 7.9 Hz, 2F); ^{13}C-NMR ($CDCl_3$): δ 13.96, 14.02, 22.5, 22.6, 25.2, 25.7, 29.2, 29.9, 31.4, 31.6, 68.1, 75.5 (t, *J* = 2.9 Hz), 75.8 (t, *J* = 3.7 Hz), 87.6, 92.1, 97.8 (t, *J* = 17.6 Hz), 99.8 (t, *J* = 2.9 Hz), 114.6, 114.7, 121.2, 124.7, 131.4, 131.7, 133.1, 138.4 (tt, *J* = 12.3, 3.0 Hz), 141.1 (ddt, *J* = 249.4, 13.9, 4.4 Hz), 147.2 (ddt, *J* = 252.5, 13.2, 3.7 Hz), 159.5; IR (KBr): ν 3039, 2954, 2857, 2210, 1597, 1520, 1492, 1250, 1122, 1019, 984, 837 cm^{-1}; HRMS: (FAB+) *m/z* $[M]^+$ calcd for $C_{34}H_{34}O_2F_4$: 550.2495; found: 550.2492.

X-Ray crystallography

Single crystals of bistolanes **1aC** and **1bA** were obtained by purification of column chromatography, followed by recrystallization (CH_2Cl_2/MeOH = 1/1), and mounted on a glass fibre. All measurements for both bistolanes were made on a diffractometer with filtered Mo-$K\alpha$ radiation (λ = 0.71075 Å) and a rotating anode generator using a VariMax with PILATUS/DW (Rigaku). All calculations were performed using the CrysAlisPro software package (Rigaku)[14] and the refinement was carried out using SHELXL-97.[15] The structures were solved by direct methods and expanded using Fourier techniques. The crystal data are deposited in the Cambridge Crystallographic Data Center (CCDC) database (CCDC 1838805 for **1aC** and 1838806 for **1bA**).

Phase transition properties

The phase transition properties of bistolanes were observed by polarizing optical microscopy (POM) using an Olympus BX51 microscope equipped with a temperature-controlled stage (Instec HCS302 microscope, hot and cold stages, and a mK1000 temperature controller). The thermodynamic parameters were determined using a differential scanning calorimeter (DSC) (SII X-DSC7000 (Seiko Instruments Inc.) or SHIMADZU DSC-60 Plus (Shimadzu)) at heating and cooling rate of 5.0 °C min^{-1}. At least three scans were conducted to confirm reproducibility.

Photophysical properties

UV-Vis absorption spectra were recorded using a JASCO V-500 absorption spectrometer. Steady-state photoluminescence spectra were obtained using a JASCO FP-8000 or a Hitachi F-7000 fluorescence spectrometer. Photoluminescence quantum yields were estimated using a calibrated integrating sphere system (JASCO).

Computation

All computations were carried out with density functional theory (DFT) using the Gaussian 09 (Rev. C.01) package.[15] Geometry optimizations were executed with the CAM-B3LYP hybrid functional[16] and 6-31G+(d) basis set. The stationary points were characterized by frequency calculations to confirm that the minimum energy structures had no imaginary frequencies.

Results and discussion

Crystal structure

Among the polyfluorinated bistolane series **1** synthesized in this study, bistolane **1aC** with two methoxy-substituents at both longitudinal molecular terminals furnished single crystals for X-ray crystallographic analysis. Figure 2 shows the top view and crystal packing structures of **1aC**.

The **1aC** crystal has the $P2_1/n$ monoclinic space group with four molecular formula per unit cell. The three aromatic rings in the bistolanes **1aA** and **1bA** were found to form co-planar structure in the crystal (Figure S1 and S2). In contrast, one of the three aromatic rings in **1aC** was twisted from the two co-planar ones by an average of approx. 60°. To check whether the crystal structure of **1aC** is the most stable one, we performed vibration frequency calculation with DFT at CAM-B3LYP/6-31+G(d) level of theory,[16,17] starting with the measured crystal structure. The calculation showed that the initial structure of **1aC** has several imaginary frequencies, indicating that it is not the most stable form but a metastable one located in a local minimum.

View Article Online
DOI: 10.1039/C8OB01497C

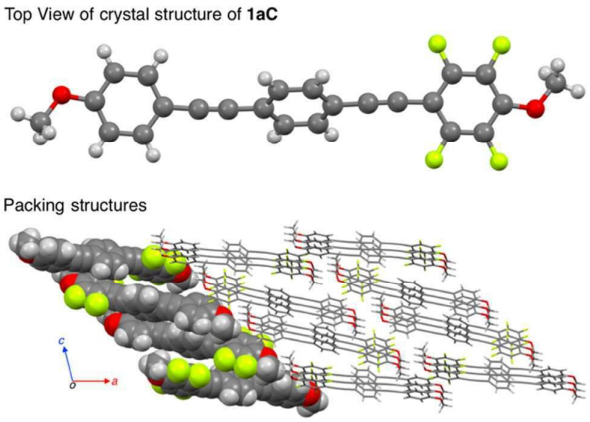

Figure 2. Molecular structure of **1aC** in crystal viewing from the top and packing structures. Four molecular units in a unit cell are drawn in space filling style.

The most stable structure, obtained from optimization at the same level, has the three aromatic rings in co-planar arrangement like the case of **1aA** and **1bA**. From the packing structures shown in Figure 2, **1aC** with the twisted form constructed relatively tight packing structures in the crystal lattice with several intermolecular interactions, e.g., π/π interaction between electron-deficient polyfluorinated aromatic ring and relatively electron-rich central benzene ring, and F/H interaction (hydrogen bonding) between fluorine on the polyfluoroaromatic ring and hydrogen in the methoxy substituent. The interatomic $C_{Ar}\cdots C_{Ar}$, $C_{Ar}\cdots H$, and $F_{Ar}\cdots H_{CH3}$ distances (for π/π interaction, CH/π interaction, and hydrogen bonding) were 329, 280, and 249 pm, respectively; all of them are shorter than the sum of the two respective van der Waals radii (C: 170 pm, H: 120 pm, F: 147 pm).[18] The multiple intermolecular interactions contribute to the close packing structure of the twisted **1aC** even in the metastable state.

Phase transition behaviour

After purification by recrystallization, the phase transition behavior of polyfluorinated bistolanes **1aB–C**, **1bB**, and **1bD** was measured by using a POM and a DSC. The measurements were repeatedly carried out to confirm the reproducibility with the same sample. The resulting phase transition sequence and transition temperature on the second heating/cooling cycle are summarized in Table 1. Details of the phase transition behaviour are shown in ESI. Figure 3 shows the optical textures of the four polyfluorinated bistolanes observed by POM in their LC phases.

All four polyfluorinated bistolanes exhibited enantiotropic LC property.[19] Among them, **1aB–C** with one or two methoxy group(s) as well as **1bD** with two hexyloxy chains showed a single LC between the optically anisotropic crystalline (Cr) phase and isotropic liquid (Iso) phases. The optical images (Figure 3) showed four-fold schlieren textures that are typical of the nematic (N) phase. The LC phase observed in **1aB–C** and **1bD** was determined as nematic phase. On the other hand, **1bB** with one hexyloxy chain and one bromine atom was found to exhibit two LC phases (LC^1 and LC^2) by POM observation.

Table 1. Phase transition behaviour of the polyfluorinated bistolane derivatives **1aB–C**, **1bB**, and **1bD**

Bistolane		Phase transition temperature [°C][a,b] (Phase transition enthalpy [kJ mol^{-1}])
1aB	Heating	Cr 192 (45.9) N 218 (0.39) Iso
	Cooling	Cr 159 (–49.1) N 220 (–0.38) Iso
1aC	Heating	Cr^1 101 (2.4) Cr^2 120 (37.7) N 250 (1.3) Iso
	Cooling	Cr^1 77 (–17.9) Cr^2 88 (–51.2) N 249 (–0.95) Iso
1bB	Heating	Cr 130 (41.0) SmA 144 (0.70) N 194 (0.75) Iso
	Cooling	Cr^1 114 Cr^2 116 (–36.0)[c] SmA 146 (–0.67) N 195 (–0.74) Iso
1bD	Heating	Cr 76 (27.2) N 182 (2.03) Iso
	Cooling	Cr^1 57 Cr^2 59 (–25.0)[c] N 185 (–0.54) Iso

[a] Abbreviations. Cr: crystalline, SmA: smectic A, N: nematic, Iso: isotropic phases. [b] Phase transition temperature was determined by DSC measurement (5.0 °C min^{-1}, N_2 atmosphere) on the 2nd cycle. [c] Indicates enthalpies during the phase transition from Cr^1 to SmA phases due to the short range of the Cr^2 phase.

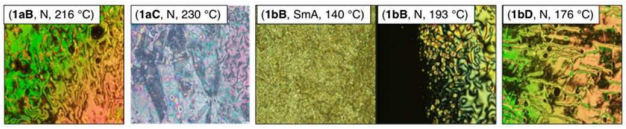

Figure 3. POM texture for polyfluorinated bistolane derivatives **1aB–C**, **1bB**, and **1bD**.

The POM results showed an oily streak texture in the LC^1 state at 140 °C on the 2nd heating, whereas the texture was dramatically switched to a schlieren image at 144 °C through a $LC^1 \rightarrow LC^2$ phase transition. Judging from the optical images, LC^1 phase at the lower temperature region may be assigned as smectic (Sm) phase,[20] while the LC^2 phase at higher temperature region can be assigned as N phase (as mentioned above).

In order to properly determine the LC^1 phase, powder X-ray diffraction measurement was carried out between 80–200 °C at 20 °C intervals during the 2nd cooling process. Selected diffraction patterns at 80 °C in Cr, 120 °C in Sm, and 180 °C in N phases are shown in Figure 4a and Figure S5. Three diffraction signals were detected at 2θ = 3.0°, 3.26°, and 5.98° in the Sm phase at 120 °C. Considering the signal at 80 °C in the Cr phase, the diffraction signal at 3.26° (d = 2.71 nm) may be attributed to an ordered structure in the Cr phase, and therefore the diffraction peaks at 3.0° (d: 2.94 nm) and 5.98° (d: 1.48 nm) can be assigned to (0 0 1) and (0 0 2) reflections, respectively, based on the interlayer structure in Sm phase. The molecular and packing structures of **1bB** were estimated from the crystal structure of **1bA** using DFT calculation. The longitudinal molecular length of **1bB** was calculated as 2.63 nm, which was shorter than the interlayer d-spacing.

View Article Online
DOI: 10.1039/C8OB01497C

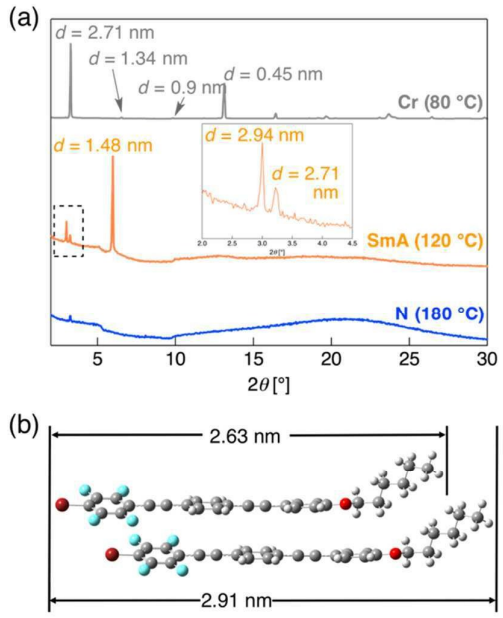

Figure 4. (a) X-ray diffraction pattern of polyfluorinated bistolane **1bB** on the 2nd cooling process. Cr: crystalline (gray), SmA: smectic A (orange), N: nematic (blue) phases. (b) Proposed molecular alignment in the SmA phase of **1bA**, estimated from crystal structures.

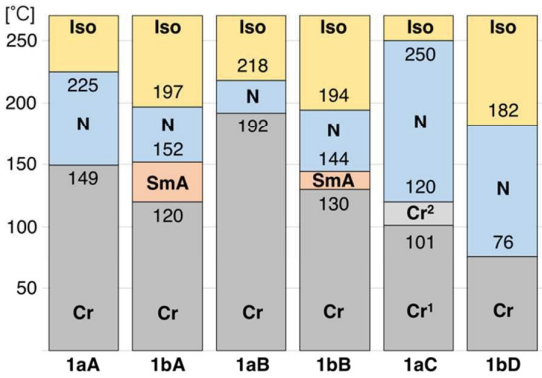

Figure 5. Phase transition sequences of different polyfluorinated bistolane analogues.

Assuming that the crystal packing structures to be similar to **1bA** which forms *syn*-dimer structure (Figure 4b), the molecular length of **1bB** in the long molecular axis (2.91 nm) for the *syn*-dimer was found to be as long as the interlayer distance in the Sm phase (2.94 nm), indicating that the LC^2 phase observed in **1bB** is a SmA phase that orderly aligns the *syn*-dimer parallel to the layer normal.

To understand the effect of substituents at the molecular terminals on the phase transition behavior, we compared the phase transition sequence of **1aB–C**, **1bB**, and **1bD** to those reported for **1aA** and **1bA** (Figure 5).

Methoxy-substituted bistolanes, e.g., **1aA–C**, showed higher melting (Cr→LC) and clearing (LC→Iso) temperature than the corresponding hexyloxy-substituted ones like **1bA–B** and **1bD**. In general, the long-alkoxy chain moiety in the **1b** series disturbs the aligned structure via a micro-Brownian motion at higher temperature, in comparison with series 1a having a short-alkoxy unit. So, these differences in phase transition temperature appear entirely reasonable.

Replacing a fluorine at one molecular terminal of **1aA** and **1bA** with a bromine atom increased the Cr→LC transition temperature by 10–43 °C, while no large difference was observed in the LC→Iso transition temperature, thereby leading to a narrower LC temperature range. According to reported literature,[21] significant increase of the Cr→LC phase transition temperature may occur due to enhanced anisotropic polarizability ($\Delta\alpha$) by changing from C_{Ar}–F to C_{Ar}–Br.[22] On the other hand, replacing a fluorine atom of **1aB** or **1bA** by a methoxy (for **1aC**) or a hexyloxy moiety (for **1bD**) dramatically stabilized the LC phase. This is due to an increased transition entropy by incorporating flexible moiety at the molecular terminal, which significantly lowers the Gibbs free energy to stabilize the LC phase.[23] As a whole, a substituent at the longitudinal molecular terminals of bistolane-type liquid crystals can strongly influence the LC characteristics (e.g., the LC phase sequence and temperature range), making such substitution a powerful tool to control the aggregated structures through phase transition.

Photoluminescence behavior

One of our main interests was the PL characteristics of the polyfluorinated bistolane derivatives, because some fluorinated bistolane analogues display intensive luminescence in their crystalline as well as solution states.[5a,11] To reveal their photophysical properties, we initially measured the UV-Vis absorption spectra and PL spectra of the four derivatives in dilute CH_2Cl_2 solution. The results are shown in Figure 6 and Figure S7, and the corresponding photophysical data are summarized in Table 2.

All four polyfluorinated bistolanes showed an absorption band in the range of 250–400 nm. From the absorption spectra in Figure 6a, the maximum absorption wavelengths (λ_{abs}) of **1aB** and **1bB** having an alkoxy unit and a bromine atom at the longitudinal molecular terminals were 336 nm. Also, identical λ_{abs} (332 nm) was observed in **1aC** and **1bD** with two alkoxy units at the longitudinal molecular terminals. The difference is attributable to the altered overall electronic structure of the molecule caused by changing substituents.

View Article Online
DOI: 10.1039/C8OB01497C

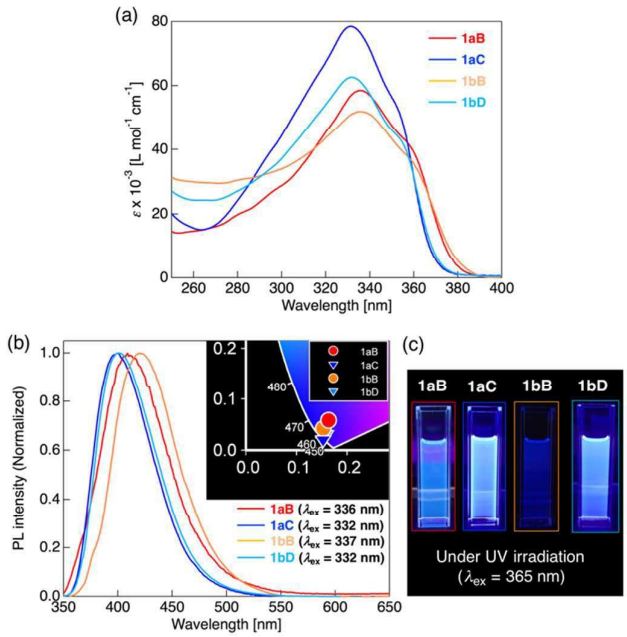

Figure 6. (a) Absorption spectra measured in 10^{-5} mol L^{-1} CH_2Cl_2 solution, (b) PL spectra in 10^{-6} mol L^{-1} CH_2Cl_2 solution (inset: CIE diagram), and (c) photographs of luminescence from the polyfluorinated bistolanes **1aB–C**, **1bC**, and **1bD** under UV irradiation (λ_{ex} = 365 nm).

Table 2. Photophysical data for the polyfluorinated bistolane derivatives **1aB–C**, **1bB**, and **1bD**.

	λ_{abs} [nm][a] (εx10^{-3} [L mol^{-1} cm^{-1}])	λ_{PL} [nm] (Φ_{PL}) in solution[b]	λ_{PL} [nm] (Φ_{PL}) in crystal[c]
1aB	336 (58.5), 356 (sh., 42.9)	409 (0.03)	425 (0.22)
1aC	332 (78.5), 349 (sh., 58.2)	400 (0.91)	399, 421 (0.36)
1bB	336 (51.9), 358 (sh., 37.2)	420 (0.07)	470 (0.06)
1bD	332 (62.6), 351 (sh., 45.2)	401 (0.90)	460 (0.19)

[a] Measured in 10^{-5} mol L^{-1} CH_2Cl_2 solution. [b] Measured in 10^{-6} mol L^{-1} CH_2Cl_2 solution. [c] Obtained by recrystallization from CH_2Cl_2/MeOH. sh. = shoulder.

Next, PL spectra of the polyfluorinated bistolane derivatives in dilute CH_2Cl_2 solution were recorded under irradiation at the respective λ_{abs} of all samples (Figure S7). The present bistolane derivatives emitted deep blue photoluminescence (Φ_{em} = 0.03–0.91) with a broad emission band at the λ_{PL} = 400–420 nm. As mentioned before, the polyfluorinated bistolanes **1** were found to possess longitudinal molecular dipole moment ($\mu_{||}$) in not only the ground (S_0) state but also the excited (S_1) state according to the DFT and time-dependent (TD) DFT calculation (Table S2). Hence, their luminescence in solution is supposed to be a radiation process through an intramolecular charge-transfer (CT) transition. **1aC** and **1bD** with two alkoxy substituents at the molecular terminals showed almost identical PL spectra, whereas a long wavelength-shift up to 20 nm was observed in the case of **1aB** and **1bB** with a bromine atom instead of alkoxy substituent. It may be due to the large CT transition characteristics induced by $\mu_{||}$ of **1aB** (5.43 D) and **1bB** (5.86 D) in the excited S_1 state.

The present polyfluorinated bistolane derivatives were found to also emit PL even in the Cr state (Figure 7 and Figure S8). In the PL spectra, only a single emission band with maximum between 425–470 nm was detected for **1aB**, **1bB**, and **1bD**; while **1aC** showed double emission bands with λ_{PL} at 399 and 421 nm, in which the shorter λ_{PL} was almost identical to that in solution state. The shorter PL band of **1aC** is supposed to originate from monomeric light emission. The reason why two emission maxima were observed in the Cr state may be due to the formation of crystalline polymorphs in **1aC**.

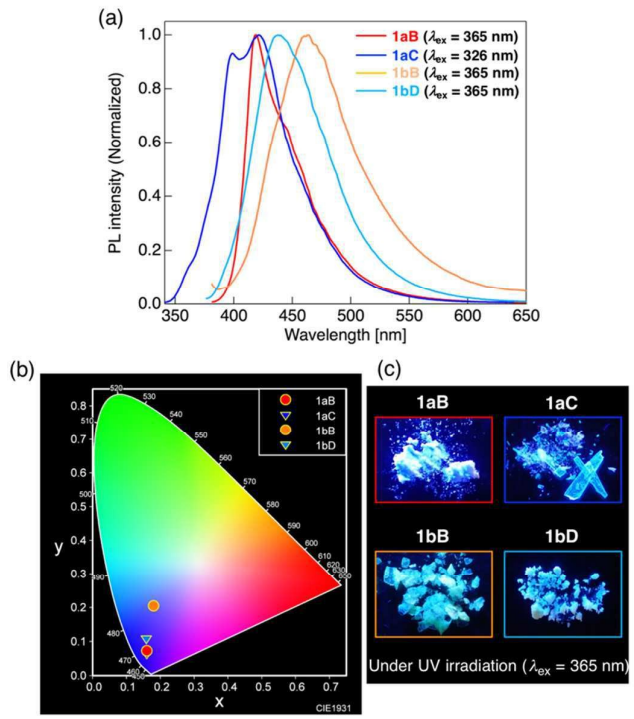

Figure 7. (a) PL spectra in crystals, (b) CIE diagram of emission color, and (c) photographs of luminescence under 365 nm UV lamp from polyfluorinated bistolanes **1aB**, **1aC**, **1bB**, and **1bD**.

As mentioned in the context of Figure 2, the crystalline **1aC** is a metastable rather than the most stable form. The crystalline polymorphous character of **1aC** permits multiple emission bands even in the Cr state. In contrast to methoxy-substituted bistolanes (**1aB** and **1aC**), the λ_{PL} in Cr state for **1bB** and **1bD** carrying a hexyloxy chain is 50–60 nm longer compared to that in solution. Considering the similarity of electronic structures among the **1b** series, the large λ_{PL} shift of **1bB** and **1bD** is likely due to different structures of the molecular aggregates, rather than electron density distribution. According to the crystal structures of **1aA** and **1bA** (Figure S1 and S2), which have one fluorine atom and one alkoxy moiety at the longitudinal molecular terminals, **1bA** possesses more types of tight stabilization by intermolecular interactions (e.g., π/π and CH/π) than in **1aA**. The intermolecular interactions worked in the molecular aggregated structures facilitates PL emission by

View Article Online
DOI: 10.1039/C8OB01497C

lowering the excitation energy. Comparing PL quantum yields (Φ_{PL}) for the present bistolanes observed in Cr state, the Φ_{PL} of **1aB** and **1bB** with a bromine atom was lower than that of **1aC** and **1bD** carrying a corresponding alkoxy substituent, which is due to the fluorescence quenching effect by bromine atom. As previously reported,[11] the Φ_{PL} of bistolane derivatives was largely attributed to the length of alkoxy chain substituted the longitudinal molecular terminal; Φ_{PL} of **1aA** with a short alkoxy moiety was higher than that of **1bA** with a long alkoxy chain owing to the suppression of non-radiative decay caused by molecular motion of alkoxy unit. With the similar manner, it is likely that the **1aB** in the present case was high Φ_{PL}, rather than the **1bB**. Furthermore, considering the PL characteristics in the Commission Internationale de l'Eclairage (CIE) diagram (Figure 7b), the present polyfluorinated bistolane derivatives showed various emission colors from deep blue to light blue by simply modulating the terminal substituent on the bistolane scaffold. Taking the similarity of electronic structures depending on the terminal substituent into consideration, the PL characteristics of the bistolanes in Cr phase seem to affect the structure of molecular aggregates altered by modulating molecular terminal substituents.

Thermoresponsive luminescence properties

Our next focus is the thermoresponsive property of the luminescence induced by thermal stimulus, because the molecular aggregates of the bistolanes can change reversibly through thermal phase transitions. The sample was prepared by placing the recrystalized bistolane sample between two quartz glass plates. **1aC** and **1bD** with two alkoxy moieties at the longitudinal molecular terminals were used as selected examples.[24] Their PL behavior was measured using a fluorescent spectrometer with heating and cooling by a home-made temperature-control unit. The temperature-dependent PL spectra are shown in Figure 8.

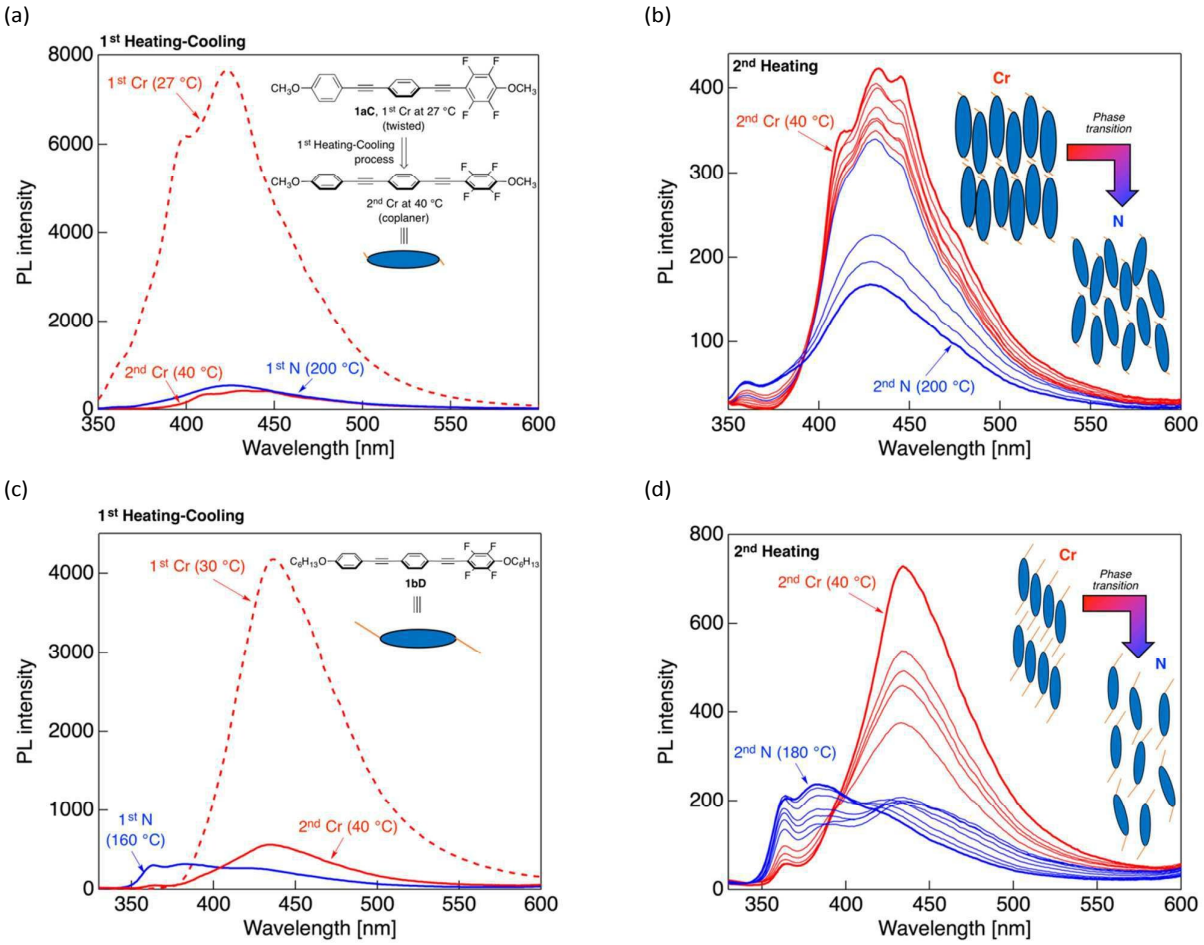

Figure 8. Temperature-dependent PL behaviour of **1aC** (λ_{ex} = 326 nm) and **1bD** (λ_{ex} = 305 nm). Red line: Cr phase, blue line: N phase. (a),(c) Selected PL spectra during 1st heating-cooling process. (b),(d) PL behavior during 2nd heating process and (insets) possible schemes of the molecular aggregated structure.

View Article Online
DOI: 10.1039/C8OB01497C

Journal Name

ARTICLE

In the 1st heating of **1aC** (Figure 8a), a dramatic decrease of PL intensity was observed from 27 °C to 200 °C, during which 1aC changed from Cr to N phase at 151 °C.[25] The sample changed back to Cr phase (denoted as 2nd Cr) by cooling to 40 °C, however the PL intensity declined significantly. Careful comparison of the spectral shapes in the 1st Cr and 2nd Cr states revealed a slight difference. As noted before, the PL spectrum in 1st Cr phase contains two emission maxima at 399 and 421 nm, whereas three emission maxima were observed at 416, 433, and 445 nm in the 2nd Cr phase after heating and cooling processes. These additional maxima may originate from a re-construction of aggregated structures, e.g., from metastable structure with a twisted conformation to the most stable form with a co-planar conformation through the fluidic N phase. After heating the sample again up to 200 °C in the 2nd heating process, as shown in Figure 8b, the PL intensity was gradually reduced, and the spectral shape also changed dramatically through the Cr→N phase transition. Before the phase transition, **1aC** in the 2nd Cr may have a co-planar structure and could therefore form order structures with multiple π/π and CH/π interactions, allowing strong PL emission. Beyond the phase transition temperature, on the other hand, the ordered structures may be disturbed and re-constructed to form loosely ordered structures with a directional anisotropy via weak interactions, which have low PL intensity. Notably, after the N→Cr phase transition in the 2nd cooling process, the spectral shape reverted up to ca. 60% of the 2nd Cr state (Figure S9). So, **1aC** clearly shows reversible thermoresponsive PL characteristics.

The other polyfluorinated bistolane **1bD** carrying two hexyloxy flexible chains behaved in a way similar to **1aC** (Figure 8c). The PL intensity of the 1st Cr gradually decreased with heating, and the spectrum became a broad emission band with several maxima in a range of 350–450 nm through Cr→N phase transition. Continuous cooling to 40 °C smoothly formed the 2nd Cr structure, whose PL spectral shape changed significantly back, showing the major emission band with λ_{PL} = 450 nm and a weak band at λ_{PL} = 360 nm. However, the PL intensity did not recover at all. Similar to the PL behavior of **1aC** under the 2nd heating process, the major PL band at 450 nm was drastically changed to plural emission bands in a high-energy region with decreasing PL intensity. Application of thermal stimulus is supposed to cause a smooth re-construction of the molecular aggregated structure, as shown in the inset of Figure 8d, from an ordered one to relaxed molecular aggregates with only an orientational regularity via weak van der Waals interactions. The drastic alteration of molecular aggregated structures is likely to lead to high-energy PL originated from monomeric light emission. In the PL behavior during the 2nd cooling process, diminished high-energy PL in the short-wavelength region and an enhanced PL band at 450 nm were observed simultaneously with repeatability. Hence, the PL characteristics of **1bD** also respond to thermal stimulus.

Conclusions

We synthesized four polyfluorinated bistolane derivatives by systematically alter the substituents at the longitudinal molecular terminals. The liquid-crystalline (LC) property of the derivatives was strongly affected by not only the electron density distribution (induced by the electron-donating or -withdrawing terminal substituents) but also the length of the flexible chain attached to the molecular terminal. Thus, an increase in the longitudinal molecular dipole moment ($\mu_{||}$) rises the melting temperature from crystalline to nematic phases, whereas the incorporation of long alkoxy chain as a flexible unit into the molecular terminal resulted in significant decrease of melting and clearing temperatures. In terms of photophysical property, the polyfluorinated bistolanes showed photoluminescence (PL) in dilute solution, crystal, as well as LC phases. The luminescence wavelength in dilute solution is largely affected by the electronic structure of the entire molecule: bistolane with large $\mu_{||}$ exhibited a shift of the emission maximum towards longer wavelength. On the other hand, their PL behavior in crystals significantly changed depending on the structures of molecular aggregates, rather than the electronic feature of the molecule. In the LC phase, the PL behavior can be tuned by altering the aggregated structures by thermal stimulus: it was remarkable that the present bistolane derivatives displayed reversible thermoresponsive PL characteristics. The thermoresponsive luminescent feature allows them to be apply for the luminescent sensing materials, and further investigations to discover light-emitting liquid-crystalline molecules are ongoing in our laboratory.

Conflicts of interest

There are no conflicts to declare.

Acknowledgements

This work was partially supported by the Asahi Glass Foundation; the Foundation for the Promotion of Ion Engineering; and JSPS KAKENHI, Grant-in-Aid for Scientific Research (C), Grand Number JP18K05262. We express our

View Article Online
DOI: 10.1039/C8OB01497C

gratitude to Profs. Osamu Tsutsumi (Ritsumeikan Univ.), Kensuke Naka and Hiroaki Imoto (Kyoto Inst. Tech.) for measuring the photophysical behaviors.

Notes and references

1 P. Raynes, in *Handbook of Liquid Crystals, 2nd Edition*, (Eds.: J. W. Goodby, P. J. Collings, T. Kato, C. Tschierske, H. Glesson, P. Raynes), Wiley-VCH Verlag GmbH & Co. KGaA, Weinheim, 2014**.**

2 (a) T. Kato, J. Uchida, T. Ichikawa, T. Sakamoto, *Angew. Chem. Int. Ed.,* 2018, **57**, 4355–4371; (b) T. Kato, J. Uchida, T. Ichikawa, T. Sakamoto, *Polym. J.,* 2018, **50**, 149–166; (c) J. C. Christopherson, F. Topic, J. Barrett, T. Friscic, *Cryst. Growth Des.,* 2018, **18**, 1245–1259; (d) B. T. Hogan, E. Kovalska, M. F. Craciun, A. Baldycheva, *J. Mater. Chem. C,* 2017, **5**, 11185–11195.

3 (a) T. D. Fink, R. H. Zha, *Macromol. Rapid Commun.,* 2018, (DOI: 10.1002/marc.201700834); (b) K. Liu, L. Zheng, C. Ma, R. Göstl, A. Herrmann, *Chem. Soc. Rev.,* 2017, **46**, 5147–5172; (c) M. Mitov, *Soft Mater.,* 2017, **3**, 4176–4209; (d) K. Iwabata, U. Sugai, Y. Seki, H. Furue, K. Sakaguchi, *Molecules,* 2013, **18**, 4703–4717.

4 B. Valeur, M. N. Berberan-Santos, *Molecular Fluorescence, Principles and Applications*, Wiley-VCH Verlag GmbH & Co. KGaA, Weinheim, 2012.

5 For references on luminescence affected by electron density distribution, see: (a) S. Yamada, M. Morita, T. Konno, *J. Fluorine Chem.,* 2017, **202**, 54–64; (b) H. Lu, L. Qiu, G. Zhang, A. Ding, W. Xu, G. Zhang, X. Wang, L. Kong, Y. Tian, J. Yang, *J. Mater. Chem. C,* 2014, **2**, 1386–1389.

6 For related reviews on luminescence affected by molecular aggregated structures, see: (a) Z. He, C. Ke, B. Z. Tang, *ACS Omega,* 2018, **3**, 3267–3277; (b) J. Mei, N. L. C. Leung, R. T. K. Kwok, J. W. Y. Lam, B. Z. Tang, *Chem. Rev.,* 2015, **115**, 1718–11940. c) R. Hu, N. L. C. Leung, B. Z. Tang, *Chem. Soc. Rev.,* 2014, **43**, 4494–4562.

7 For references on pH-sensitive luminescent molecules, see: (a) R. Goter, P. Ashokkumar, M. Hecht, K. Keil, K. Rurack, *Anal. Chem.,* 2017, **89**, 8437–8444; (b) R. Chen, H. Jiang, H. Gu, Q. Zhou, J. Wu, D. Chen, J. Zhang, *Chem. Commun.,* 2015, **51**, 12220–12223.

8 For references on metal ion-sensitive luminescent molecules, see: (a) C. Pan, K. Wang, S. Ji, H. Wang, Z. Li, H. He, Y. Huo, *RSC. Adv.,* 2017, **7**, 36007–36014; (b) T. Schwarze, J. Riemer, S. Eidner, H.-J. Holdt, *Chem. Eur. J.,* 2015, **21**, 11306-11310; (c) S. Sumalekshmy, C. J. Fahrni, *Chem. Mater.,* 2011, **23**, 483–500.

9 For references on thermosresponsive luminescent molecules, see: (a) T. Xia, L. Wang, Y. Qu, Y. Rui, J. Cao, Y. Hu, J. Yang, J. Wu, J. Xu, *J. Mater. Chem. C,* 2016, **4**, 5696–5701; (b) A.C. Benniston, G. Copley, A. Harriman, R. Ryan, *J. Mater. Chem.,* 2011, **21**, 2601–2608.

10 For references on luminescent switching induced by mechanical stress, see: (a) C. Wang, Z. Li, *Mater. Chem. Front*., 2017, **1**, 2174–2194. (b) Y. Sagara, S. Yamane, M. Mitani, C. Weder, T. Kato, *Adv. Mater.,* 2016, **28**, 1073–1095.

11 S. Yamada, K. Miyano, T. Konno, T. Agou, T. Kubota, T. Hosokai, *Org. Biomol. Chem.,* 2017, **15**, 5949–5958.

12 For related studies about temperature-responsive luminescent liquid crystalline materials, see: (a) J. A. H. P. Sol, V. Dehm, R. Hecht, F. Würthner, A. P. H. J. Schenning, M. G. Debije, *Angew. Chem. Int. Ed.*, 2018, **57**, 1030–1033. (b) K. Nabeya, T. Muraoka, N. Hoshino, M. Aizawa, T. Kajitani, T. Akutagawa, A. Shishido, T. Fukushima, K. Kinbara, *Mater. Chem. Front.*, 2018, **2**, 969–974. (c) M. Alaasar, S. Poppe, Q. Dong, F. Liu, C. Tschierske, *Angew. Chem. Int. Ed.*, 2017, **56**, 10801–10805.

13 C. B. Aakeröy, P. D. Chopade, J. Desper, *Cryst. Growth Des.,* 2013, **13**, 4145–4150.

14 *CrysAlisPro, Data Collection and Processing Software*; Rigaku Corp.: Tokyo, Japan (2015).

15 G. M. Sheldrick, *Acta Crystallogr., Sect. A: Found. Crystallogr.,* 2008, **64**, 112–122.

16 M. J. Frisch, G. W. Trucks, H. B. Schlegel, G. E. Scuseria, M. A. Robb, J. R. Cheeseman, G. Scalmani, V. Barone, B. Mennucci, G. A. Petersson, H. Nakatsuji, M. Caricato, X. Li, H. P. Hratchian, A. F. Izmaylov, J. Bloino, G. Zheng, J. L. Sonnenberg, M. Hada, M. Ehara, K. Toyota, R. Fukuda, J. Hasegawa, M. Ishida, T. Nakajima, Y. Honda, O. Kitao, H. Nakai, T. Vreven, J. A. Montgomery, Jr., J. E. Peralta, F. Ogliaro, M. Bearpark, J. J. Heyd, E. Brothers, K. N. Kudin, V. N. Staroverov, R. Kobayashi, J. Normand, K. Raghavachari, A. Rendell, J. C. Burant, S. S. Iyengar, J. Tomasi, M. Cossi, N. Rega, J. M. Millam, M. Klene, J. E. Knox, J. B. Cross, V. Bakken, C. Adamo, J. Jaramillo, R. Gomperts, R. E. Stratmann, O. Yazyev, A. J. Austin, R. Cammi, C. Pomelli, J. W. Ochterski, R. L. Martin, K. Morokuma, V. G. Zakrzewski, G. A. Voth, P. Salvador, J. J. Dannenberg, S. Dapprich, A. D. Daniels, Ö. Farkas, J. B. Foresman, J. V. Ortiz, J. Cioslowski and D. J. Fox, *Gaussian 09W*, *Revision D.01*, Gaussian, Inc., Wallingford CT, 2013.

17 (a) T. Yanai, D. P. Tew, N. C. Handy, *Chem. Phys. Lett.,* 2004, **393**, 51–57; (b) K. Okuno, Y. Shigeta, R. Kishi, M. Nakano, *Chem. Phys. Lett.,* 2013, **585**, 201–206.

18 A. Bondi, *J. Phys. Chem.* **1964**, *68*, 441–451.

19 For references on the bistolane-based liquid crystalline molecules, see: (a) Y. Arakawa, H. Tsuji, *Mol. Cryst. Liq. Cryst.,* 2017, **647**, 422–429; (b) Y. Arakawa, S. Kang, H. Tsuji, J. Watanabe, G. Konishi, *RSC Adv.,* 2016, **6**, 92845–92851; (c) Y. Arakawa, S. Kang, H. Tsuji, J. Watanabe, G. Konishi, *RSC Adv.,* 2016, **6**, 16568–16574; (d) D. Weglowsk, P. Kula, J. Herman, *RSC Adv.,* 2016, **6**, 403–408; (e) Y. Arakawa, H. Kuwahara, K. Sakajiri, S. Kang, M. Tokita, G. Konishi, *Liq. Cryst.,* 2015, **42**, 1419–1427.

20 The optical image was observed to change from bright-field to the dark-field image after applying shear stress, which can be usually observed when the molecular alignment switches from homogenous to homeotropic arrangements; the texture switching behavior is a typical observation in the SmA phase, not the SmC phase.

21 For references on effect of substituent at the molecular terminal on the nematic LC behaviour, see: (a) W. H. De Jeu, J. van der Veen, *Mol. Cryst. Liq. Cryst.,* 1977, **40**, 1–17; (b) J. van der Veen, *J. Phys. Colloques,* 1975, **36**, C1-375–C1-377.

22 Reported anisotropic polarizabilities ($\Delta\alpha$) of C_{Ar}–Br and C_{Ar}–F bonds are 3.9 and 0.5 $Å^3$, respectively.

23 (a) Y. Yamamura, T. Adachi, T. Miyazawa, K. Horiuchi, M. Sumita, M. Massalska-Aroddz, S. Urban, K. Saito, *J. Phys. Chem. B,* 2012, **116**, 9255–9260; (b) K. Horiuchi, Y. Yamamura, R. Pełka, M. Sumita, S. Yasuzuka, M. Massalska-Arodz, K. Saito, *J. Phys. Chem. B,* 2010, **114**, 4870–4875.

24 Temperature-dependent PL spectra of **1aA** and **1bA** with one fluorine atom and one alkoxy chain are also shown in Figure S9 in ESI.

25 Phase transition temperatures for all polyfluorinated bistolanes are summarized in Table S4 in ESI.

View Article Online
DOI: 10.1039/C8OB01497C

Table of contents graphics

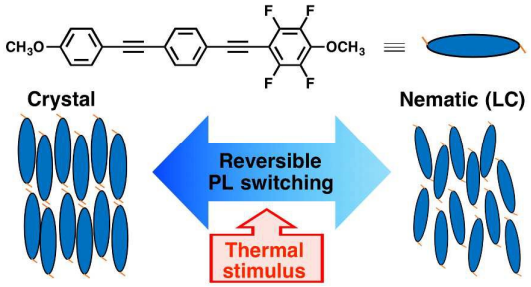

Thermoresponsive luminescent materials based on polyfluorinated bistolanes were developed and found to show reversible PL switching by applying thermal stimulus.